© IWA Publishing 2020
1228

Water Practice & Technology Vol 15 No 4
doi: 10.2166/wpt.2020.093

# Utilization of iron sludge resulted from electro-coagulation in heterogeneous photo-Fenton process

Mahmoud Samy[a,b,*], Mohamed Gar Alalm[a,c] and Mohamed Mossad[a]

[a] Department of Public Works Engineering, Faculty of Engineering, Mansoura University, Mansoura 35516, Egypt

[b] Environmental Engineering Department, Egypt-Japan University of Science and Technology (E-Just), New Borg El Arab City, Alexandria 21934, Egypt

[c] Department of Civil and Environmental Engineering, Tokyo Institute of Technology, Meguro-ku, Tokyo 152-8552, Japan

*Corresponding author. E-mail: mahmoud.samy@ejust.edu.eg

## Abstract

The iron sludge generated from an electrocoagulation process was employed for the degradation of phenol through photo-Fenton process instead of iron salts. The morphology, functional groups and chemical composition of the iron sludge were investigated using scanning electron microscopy, Fourier infrared spectroscopy, and energy-dispersive X-ray spectroscopy. The effects of iron dose, $H_2O_2$ concentration, reaction time and initial concentration of phenol on photo-Fenton process performance were studied. The degradation efficiency of phenol reached 100% in the case of light compared to 68.6% in the case of dark reaction at pH of 3, iron dose of 150 mg/L and $H_2O_2$ concentration of 1.5 g/L. The degradation efficiencies of phenol were 100%, 71.3 and 51% at initial phenol concentrations of 50 mg/L, 100 mg/L and 150 mg/L, respectively. The expected cost for the treatment of one cubic meter of the contaminated wastewater was estimated to be 0.6224 $/m$^3$.

**Key words:** iron sludge, operating parameters, phenol, photo-Fenton, wastewater

## Highlights

- Iron sludge was treated and employed as a catalyst in photo-Fenton process.
- High degradation efficiency of phenol was attained.
- The phenol degradation was improved under illumination.
- Using iron sludge in photo-Fenton process reduced the total costs.

## Graphical Abstract

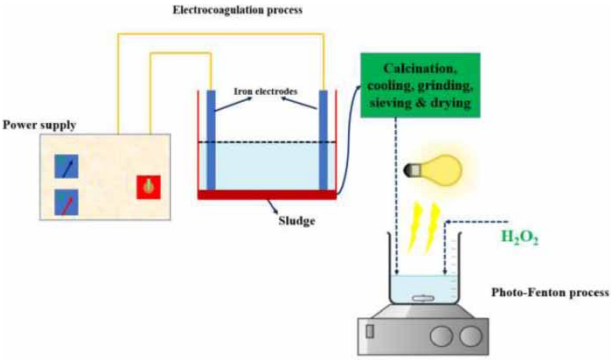

Water Practice & Technology Vol 15 No 4
doi: 10.2166/wpt.2020.093

## INTRODUCTION

Phenol is frequently detected in ground and surface water through the discharge of effluents from food processing, resins and oil refinery industries (Gar Alalm *et al.* 2016). The existence of phenol in water streams even at low concentrations has attracted wide attention due to its adverse impact on human public health and aquatic life (Sánchez-Rodríguez *et al.* 2018). Moreover, the development of a new generation of bacteria that are capable of resisting a broad range of antibiotics and disinfectants may take place due to the presence of phenol in the aquatic environment (Jiang *et al.* 2019). The low biodegradability, as well as the toxicity of phenol, complicate its removal through conventional biological treatment processes (Samy *et al.* 2020a, 2020b). Moreover, physio-chemical processes are not effective to remove phenol, as they transform the non-biodegradable organics to sludge. The generation of high amounts of sludge requires post-treatment (Samy *et al.* 2019). Therefore, researchers have focused on the development of new techniques that have the potential to degrade bio-resistant pollutants to harmless intermediates. Recently, advanced oxidation processes (AOPs) have been employed for the removal of bio-recalcitrant contaminants through the generation of reactive species such as the hydroxyl radical ($OH^{\cdot}$) that are able to oxidize the bio-resistant pollutants to simpler by-products (Gar Alalm *et al.* 2018; Samy *et al.* 2020c). AOPs such as photocatalytic degradation (Shi *et al.* 2019; Samy *et al.* 2020d), Fenton reaction (Gümüş & Akbal 2016), photo-Fenton process (Wang *et al.* 2017) and ozonation (Wei *et al.* 2020) have been investigated for the degradation of phenol. Among AOPs, the photo-Fenton process has proved a high degradation performance for various refractory pollutants. The generation of hydroxyl radicals in the Fenton process happens via the reaction of ferrous ions ($Fe^{2+}$) with hydrogen peroxide ($H_2O_2$) (Wang *et al.* 2019). The aforementioned reaction results in the oxidation of $Fe^{2+}$ to ferric ions ($Fe^{3+}$). In the photo-Fenton process, extra hydroxyl radicals can be generated, as the light reduces $Fe^{3+}$ to $Fe^{2+}$ to react again with $H_2O_2$ (Grassi *et al.* 2020). Moreover, the $H_2O_2$ can be decomposed by light to hydroxyl radicals (Wang *et al.* 2018). The additional hydroxyl radicals generated in the photo-Fenton process give this process its superiority over other traditional Fenton reactions.

Electrocoagulation (EC) is one of the previously mentioned physio-chemical processes that produce considerable quantities of sludge. The sludge generated from EC using iron electrodes contains iron hydroxides which can be employed as a catalyst in the photo-Fenton process. Therefore, in this study, the sludge taken from the EC process was utilized in the photo-Fenton reaction to overcome the problem of sludge related to the EC process and minimize the cost of the photo-Fenton process.

In this study, the iron sludge from the EC process was employed in the photo-Fenton process instead of iron salts. The morphology, chemical composition and functional groups of the iron sludge were studied using scanning electron microscopy (SEM), energy dispersive X-ray (EDX) spectroscopy and Fourier transform infrared spectroscopy (FTIR). The effects of reaction time, initial concentration of phenol, $H_2O_2$ concentration and the iron sludge dose were investigated. The degradation kinetics of phenol were studied. Moreover, estimation of the expected cost per cubic meter ($m^3$) of the industrial wastewater containing phenol was carried out.

## MATERIALS AND METHODS

### Materials

Phenol ($C_6H_5OH$, 99.5%) was purchased from Sigma Aldrich. Methanol ($CH_3OH$), hydrogen peroxide ($H_2O_2$), sodium hydroxide (NaOH) and hydrochloric acid (HCl) were purchased from Merck. All chemicals were used directly without any modifications.

Water Practice & Technology Vol 15 No 4
doi: 10.2166/wpt.2020.093

### Preparation of iron sludge

The sludge generated from the EC process was calcined at 500 °C for 4 h to remove all organics. Then, the sludge was cooled at room temperature for 24 h. After cooling, the sludge was ground and sieved with a 100 mesh sieve to ensure fine particles. The sludge was then vigorously washed with water to remove impurities. The final step was the drying of the washed sludge in an oven at 105 °C for 24 h.

### Experimental procedures

All experiments were conducted in a photo-Fenton reactor. The reactor comprises a 250 mL Pyrex beaker containing 100 mL of the phenol solution at the desired concentration. A metal halide lamp (400 W, Philips) was set at 15 cm from the solution surface. The wavelength and photon flux of the lamp were 510 nm and 220 μW $cm^{-2}$, respectively. Samples were withdrawn every 30 min and filtered before the analysis. The influences of various operating parameters were studied by changing the $H_2O_2$ concentration from 0 g/L to 1.5 g/L, initial phenol concentration from 50 mg/L to 150 mg/L and iron concentration from 0 mg/L to 200 mg/L.

### Analytical methods

The concentration of phenol was quantified using HPLC (Agilent 1200 series). All samples were filtered using a syringe filter with a porosity of 0.2 μm and then injected to the C-18 column. To detect the signal peak of phenol, a mixture of methanol and ultrapure water with ratios of 88 and 12%, respectively, was used as a mobile phase. The injection volume, temperature and flow rate were 25 μL, 40 °C and 0.9 mL/min. The detection wavelength was 270 nm.

The morphology of iron sludge was studied using scanning electron microscopy (SEM, Joel JEM 2100, Japan). Fourier transform infrared spectroscopy (FTIR, Nicolet IS 10, USA) was used to specify the functional groups of the iron sludge. The chemical composition of iron sludge was defined using energy dispersive X-ray (EDX, JEOL JSM-6510LV, Japan) spectroscopy.

## RESULTS AND DISCUSSION

### Characterization of iron sludge

The morphology of iron sludge particles is spherical as shown in Figure 1(a). The SEM image demonstrated the small size of iron sludge particles suggesting a high surface area. The well-crystalline surface, as well as the existence of some floccules from the EC process, are confirmed by SEM image. The EDX pattern in Figure 1(b) confirmed the existence of Fe, C, O and Ca. The presence of $Ca^{2+}$ ions in the sludge components may be due to the precipitation of $Ca^{2+}$ ions during the EC process by the reaction with carbonate anions. The presence of other elements (Si and Cu) may be due to the composition of the imaging grid (Bakre *et al.* 2016). Figure 1(c) shows the FTIR spectra of the iron sludge. The peaks at 463 $cm^{-1}$ and 544 $cm^{-1}$ are attributed to the Fe-O stretching vibration modes insuring the existence of iron hydroxides (Novoselova 2016). The bands at 1,630 $cm^{-1}$ and 3,423 $cm^{-1}$ are ascribed to the O-H stretching modes (Omwene & Kobya 2018). Moreover, the peaks in the region from 1,600 $cm^{-1}$ to 1,650 $cm^{-1}$ are assigned to H-O-H bending mode (Novoselova 2016). The bands observed at 2,927 $cm^{-1}$, 2,966 $cm^{-1}$ and 1,382 $cm^{-1}$ are allocated to bending modes of C- H that come from the residual organics in the iron sludge (Samy *et al.* 2019).

Water Practice & Technology Vol 15 No 4
doi: 10.2166/wpt.2020.093

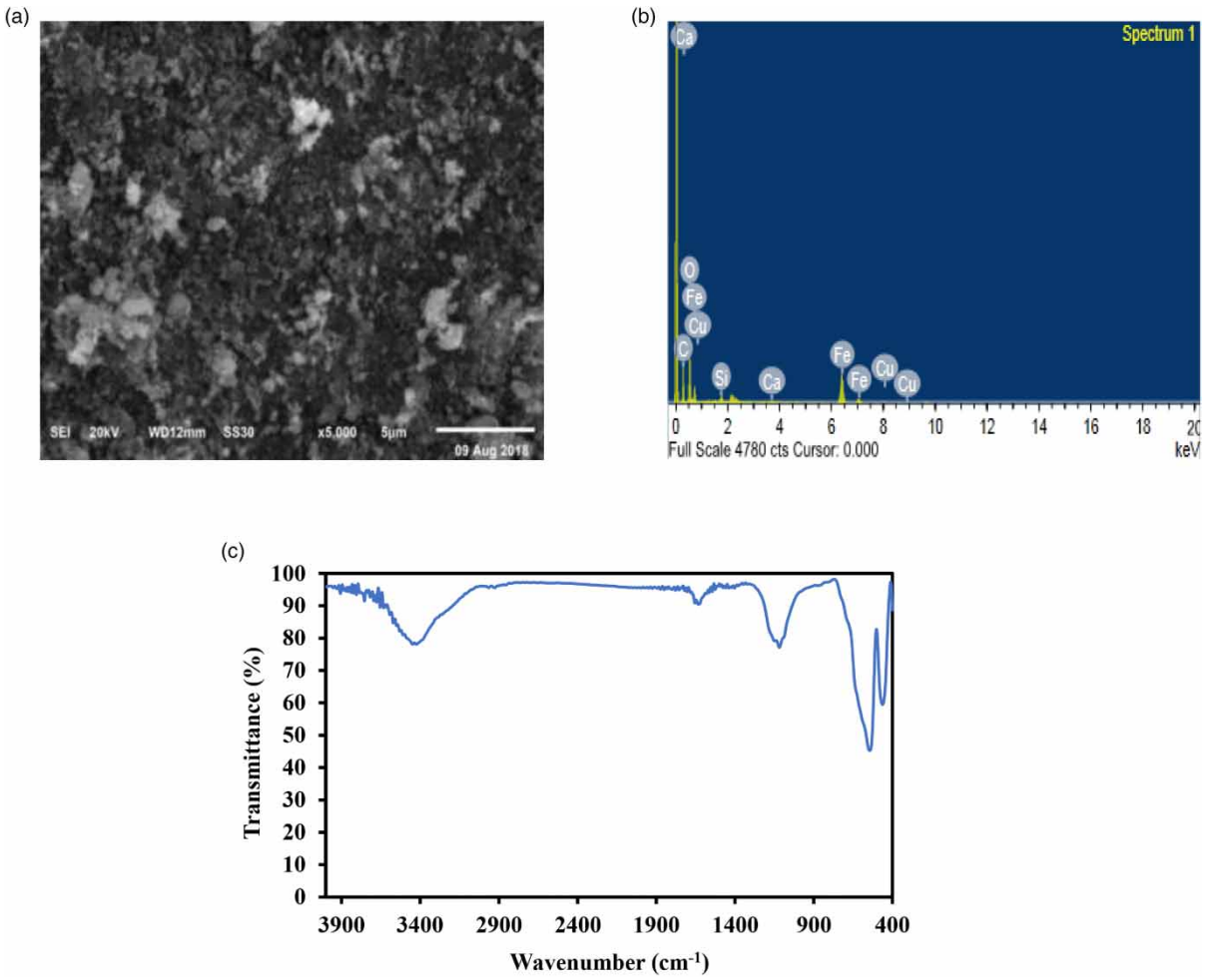


**Figure 1** | Characterization of iron sludge (a) SEM image, (b) EDX pattern and (c) FTIR spectra.

### Effect of illumination time, pH and light on the degradation efficiency of phenol

The degradation rates of phenol were high in the early stages of the reaction, then the degradation rates started to decline due to the consumption of hydroxyl radicals. The hydroxyl radicals were consumed in the removal of phenol and its intermediates. During the degradation of phenol, aromatic intermediates such as benzoquinone, catechol (benzene-1,2-diol), hydroquinone (1,4-Dihydroxybenzene) can be generated (Gar Alalm *et al.* 2016). Then, the continuous oxidation of the generated by-products converts the intermediates to simpler by-products such as maleic, oxalic, acetic, and glycol acids and finally transformed to $CO_2$ and $H_2O$ (Gar Alalm *et al.* 2016). The oxidation of these intermediates via hydroxyl radicals reduced the hydroxyl radicals available for the degradation of phenol and consequently, the degradation rates of phenol declined with time.

The photo-Fenton process is greatly affected by pH. Previous studies confirmed the high degradation performance of the photo-Fenton process in acidic conditions, so the preliminary experiments were performed at pH values of 2, 3, 4 and 5 to specify the optimum pH value (Radwan *et al.* 2018). At pH higher than 3, the degradation efficiency declined due to the formation of $Fe(OH)_3$ resulting in the reduction of $Fe^{+3}$ ions (Shokri 2018). Moreover, the continuous generation of $Fe^{+2}$ can be inhibited, leading to lower photodegradation efficiency of phenol (Rosales *et al.* 2012). At a pH value of 2, $H_2O_2$ employs as a hydroxyl radicals deactivator (Radwan *et al.* 2018). Furthermore, oxonium ions probably exist in the case of low values of pH resulting in the

Water Practice & Technology Vol 15 No 4
doi: 10.2166/wpt.2020.093

increase of $H_2O_2$ stability (Xu *et al.* 2009). The increase of $H_2O_2$ stability reduces the probability of the reaction between $H_2O_2$ and $Fe^{2+}$. The results showed that high degradation efficiency of phenol was achieved at a pH of 3 which is in accordance with our previous study (Radwan *et al.* 2018). Therefore, all the following experiments were conducted at pH of 3.

The degradation efficiencies of phenol were 68.6 and 100% in the case of absence and presence of light, respectively, at pH of 3, $H_2O_2$ concentration of 1.5 g/L, initial phenol concentration of 50 mg/L and iron dose of 150 mg/L, as shown in Figure 2. The presence of a light source results in the generation of additional hydroxyl radicals through the reduction of $Fe^{3+}$ to $Fe^{2+}$ as depicted in Equation (1). Moreover, the light source participates in the split of $H_2O_2$ to $2OH^{\cdot}$ according to Equation (2).

$$Fe^{3+} + h\nu \rightarrow Fe^{2+} + OH^{\cdot} \quad (1)$$

$$H_2O_2 + h\nu \rightarrow 2OH^{\cdot} \quad (2)$$

In the case of dark, hydroxyl radicals can be only generated from the reaction of $Fe^{2+}$ with $H_2O_2$ as shown in Equation (3).

$$Fe^{2+} + H_2O_2 \rightarrow Fe^{3+} + OH^{\cdot} + OH^{-} \quad (3)$$

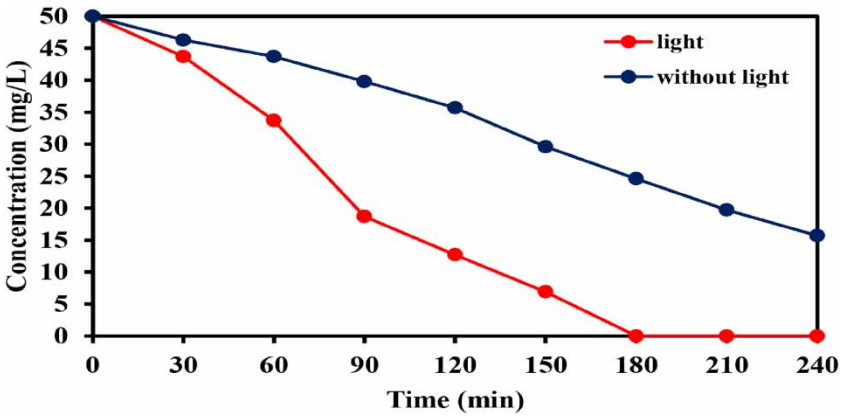


**Figure 2** | Effect of light on the degradation efficiency of phenol, pH of 3, $H_2O_2$ concentration of 1.5 g/L, iron dose of 150 mg/L, initial phenol concentration of 50 mg/L and reaction time of 240 min.

### Effect of $H_2O_2$ concentration

The increase of $H_2O_2$ concentration from 0 g/L to 1.5 g/L, as shown in Figure 3, enhanced the degradation efficiency from 12.6% to 100% at pH of 3, iron dosage of 1.5 g/L and initial phenol concentration of 50 mg/L due to the rise of hydroxyl radicals generated from the reaction between $Fe^{+2}$ and $H_2O_2$ as well as the hydroxyl radicals released from the decomposition of $H_2O_2$ by light. It was noticed that the degradation of phenol using 1 g/L of $H_2O_2$ was 94.5% and the degradation efficiency was 100% at an $H_2O_2$ concentration of 1.5 g/L. The increase of $H_2O_2$ concentration above 1 g/L did not significantly improve the degradation efficiency due to the formation of hydroperoxyl radicals (Tolba *et al.* 2020). The oxidation ability of hydroperoxyl radicals is lower than hydroxyl radicals (Zamora *et al.* 2006). Moreover, higher concentrations of hydrogen peroxide may employ as a scavenger of hydroxyl radicals (Xie *et al.* 2016). Furthermore, the reaction of hydrogen peroxide with hydroxyl radicals instead of phenol may take place at high concentrations of $H_2O_2$ (Elmolla & Chaudhuri 2010).

Water Practice & Technology Vol 15 No 4
doi: 10.2166/wpt.2020.093

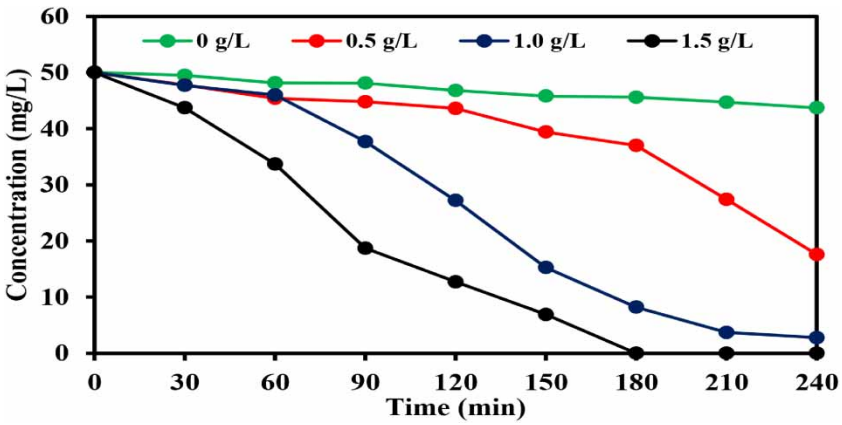


**Figure 3** | The degradation efficiencies of phenol at various concentrations of $H_2O_2$, pH of 3, iron dose of 150 mg/L, initial phenol concentration of 50 mg/L and reaction time of 240 min.

### Effect of iron sludge dose

The rise of iron dose from 0 mg/L to 150 mg/L improved the degradation efficiency from 59.6% to 100% due to the increase of hydroxyl radicals generated, as shown in Figure 4. The degradation efficiency of phenol was 100% after 240 min at an iron dose of 125 mg/L, pH of 3 and initial phenol concentration of 50 mg/L, whereas the removal efficiency of phenol was 100% after 180 min at an iron dose of 150 mg/L, pH of 3 and initial phenol concentration of 50 mg/L. However, the raising of iron dose above 150 mg/L may have a reverse impact on the degradation efficiency of phenol. The decline of degradation efficiency may be due to the consumption of iron in the coagulation of fine particles (Adel *et al.* 2020). Moreover, higher doses of iron lead to the high turbidity in the solution hindering the light to reduce $Fe^{3+}$ and decompose $H_2O_2$ (Shokri 2018).

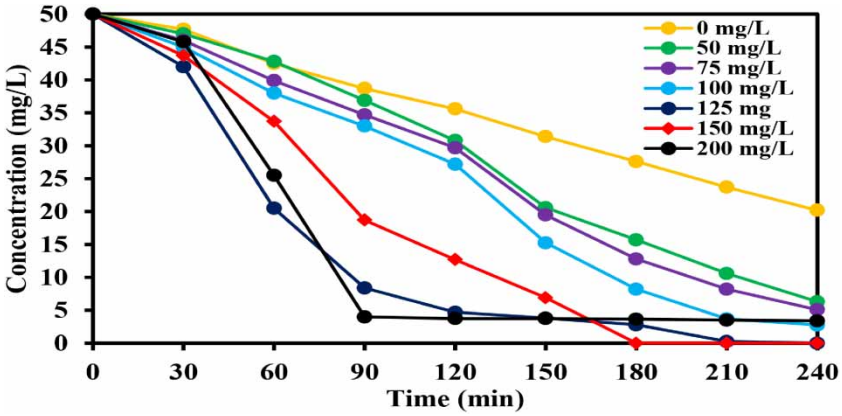


**Figure 4** | The degradation efficiencies of phenol at various doses of iron, pH of 3, $H_2O_2$ concentration of 1.5 g/L, initial phenol concentration of 50 mg/L and reaction time of 240 min.

### Effect of the initial concentration of phenol

The effect of the initial concentration of phenol on the degradation efficiency of phenol is shown in Figure 5(a). The removal efficiencies of phenol were 100%, 71.3 and 51% at initial phenol concentrations of 50 mg/L, 100 mg/L and 150 mg/L, respectively at pH of 3, iron dose of 150 mg/L and $H_2O_2$ concentration of 1.5 g/L. The increase of initial phenol concentration decreased the degradation efficiency of phenol, as the number of hydroxyl radicals generated remained constant

Water Practice & Technology Vol 15 No 4
doi: 10.2166/wpt.2020.093

regardless of the initial concentration of phenol (Saber *et al.* 2014). Therefore, the reaction time should be extended in the case of higher concentrations of phenol to achieve the desired removal.

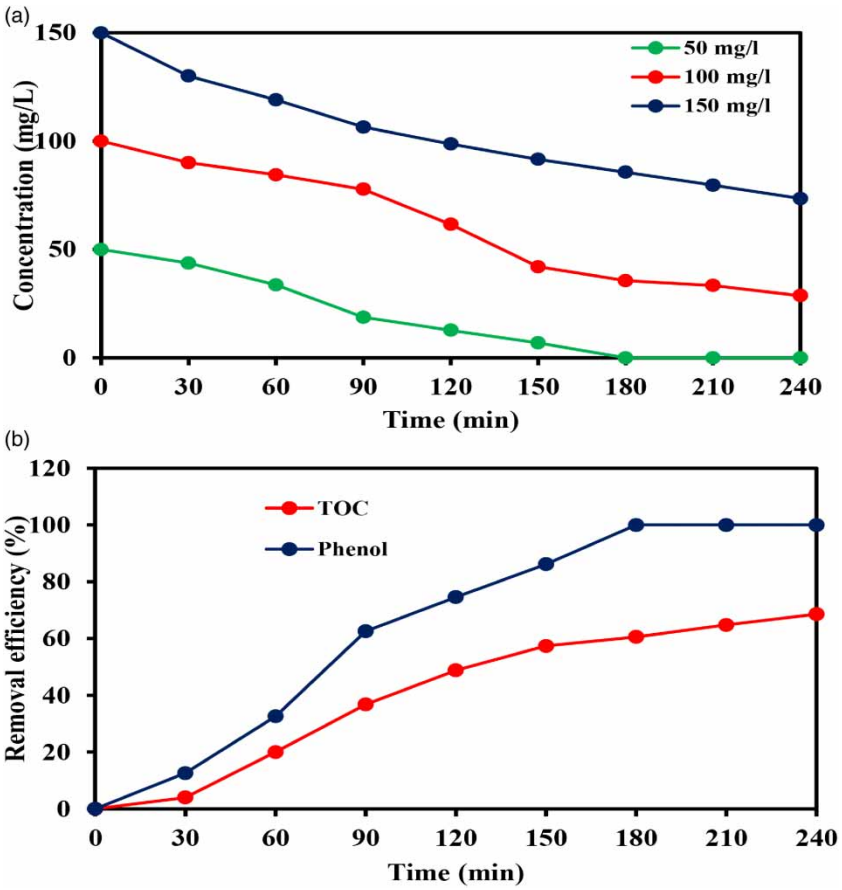


**Figure 5** | The effect of initial concentration of phenol on the degradation efficiency of phenol (a) and the TOC removal efficiency of phenol (b), pH of 3, $H_2O_2$ concentration of 1.5 g/L, initial phenol concentration of 50 mg/L, iron dose of 150 mg/L and reaction time of 240 min.

The TOC removal efficiency of 50 mg/L of phenol was 68.6%, as shown in Figure 5(b). The TOC mineralization rate was high at the beginning of the reaction, then started to decrease due to the rise of generated intermediates. The previously mentioned by-products increase the TOC concentration in the solution. However, the TOC values continued to decrease, as the degradation rate remained higher than the by-products generation rate. To achieve a high mineralization percentage of TOC, the reaction time should be extended.

### Degradation kinetics of phenol

The Langmuir-Hinshelwood model was employed to determine the degradation rates of various concentrations of phenol, as shown in Figure 6. Equation (4) describes the relationship between the initial concentration of phenol ($C_o$), the phenol concentration at time (t) (C) and the reaction rate (K):

$$\mathrm{Ln}\left(\frac{C_o}{C}\right) = K\ t \tag{4}$$

The degradation rates were 0.0104, 0.0051 and 0.0031 at initial phenol concentrations of 50 mg/L, 100 mg/L and 150 mg/L, respectively. The $R^2$ values were 0.92, 0.94 and 0.97 in the case of initial phenol concentrations of 50 mg/L, 100 mg/L and 150 mg/L, respectively.

Water Practice & Technology Vol 15 No 4
doi: 10.2166/wpt.2020.093

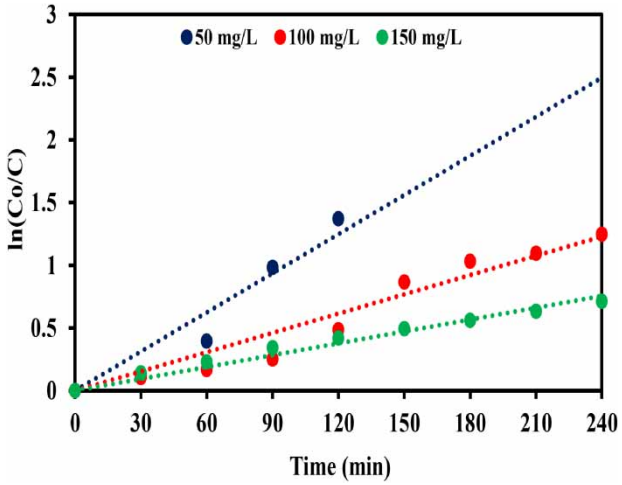


**Figure 6** | Degradation kinetics of phenol at different concentrations of phenol, pH of 3, $H_2O_2$ concentration of 1.5 g/L, iron dose of 150 mg/L and reaction time of 240 min.

### The estimation of photo-Fenton process cost

The total cost of the photo-Fenton process (TC) is the sum of the operating cost (OC) and amortization cost (AC). The total cost varied according to the amount of treated wastewater and the capacity of the reactor. The reactor volume is assumed to be 10 $m^3$ and the reactor body is made of concrete with a lifetime (n) of 25 years. It is assumed that the industrial facility works 300 days per year (D) and 12 h per day ($t_w$). The wastewater is considered to be treated in continuous batches. The time of one batch ($t_b$) is the summation of reaction time (1.5 h) besides the ripening, filling and emptying time of the reactor (30 min), so $t_b$ is assumed to be 2 h. The AC comprises the cost of reinforced concrete, mixers and other required equipment. The amortization cost can be estimated according to our previous study (Gar Alalm & Nasr 2018). The average amortization cost per cubic meter of treated wastewater is 0.12 \$/$m^3$ based on an interest rate of 6% and current amortization cost ($C_{p0}$) of 1,800 \$/$m^3$. The OC involves the cost of chemicals (Cch), maintenance cost and energy consumption cost. The cost of operating staff was not considered in this study for simplicity. The chemical cost (Cch) includes the cost of $H_2O_2$, HCl, NaOH and other necessary chemicals. The energy consumption cost is estimated according to our previous work (Gar Alalm *et al.* 2015). The maintenance cost is assumed to be 2% of AC. The OC and TC can be estimated as shown in Equations (5) and (6):

$$OC = C_{ch} + EC + 0.02 \times AC \quad (5)$$

$$TC = OC + AC \quad (6)$$

It is estimated that the cost of chemicals and energy consumption cost are 0.2 \$/$m^3$ and 0.3 \$/$m^3$, respectively. Therefore, the operating cost including maintenance cost is 0.5024 \$/$m^3$ and the total cost is .6224 \$/$m^3$.

## CONCLUSIONS

- High degradation efficiency of phenol was achieved using iron sludge from the EC process.
- The characterization of iron sludge confirmed the small size of sludge particles and the existence of iron hydroxides.
- The existence of light plays a major role in the enhancement of degradation efficiency of phenol.
- The increase of $H_2O_2$ concentration above 1 g/L did not greatly improve the degradation efficiency.

Water Practice & Technology Vol 15 No 4
doi: 10.2166/wpt.2020.093

- The raising of the iron dose above 150 mg/L decreased the degradation efficiency of phenol.
- The degradation efficiency of phenol went down by increasing the initial concentration of phenol.
- The degradation of phenol followed the pseudo-first order model.
- The use of sludge from the EC process instead of iron salts in the photo-Fenton process reduced the cost of the treatment of one cubic meter of the contaminated wastewater and reuse of iron sludge decreases the environmental burden.

## ACKNOWLEDGEMENT

The experimental work was supported by the Science and Technology Development Fund (STDF) (project No 26279). The second author is supported by a postdoctoral fellowship granted by the Japan Society for the Promotion of Science (JSPS) (Grant No: 19F19349).

## CONFLICT OF INTEREST

The authors declare that there are no conflicts of interest in this work and its publication.

## DATA AVAILABILITY STATEMENT

All relevant data are included in the paper or its Supplementary Information.

## REFERENCES

Adel, A., Gar Alalm, M., El-Etriby, H. k. & Boffito, D. C. 2020 Optimization and mechanism insights into the sulfamethazine degradation by bimetallic ZVI/Cu nanoparticles coupled with $H_2O_2$. *Journal of Environmental Chemical Engineering* **8**(5), 104341. https://doi.org/10.1016/j.jece.2020.104341.

Bakre, P. V., Volvoikar, P. S., Vernekar, A. A. & Tilve, S. G. 2016 Influence of acid chain length on the properties of $TiO_2$ prepared by sol-gel method and LC-MS studies of methylene blue photodegradation. *Journal of Colloidal and Interface Science* **474**, 58–67. http://dx.doi.org/10.1016/j.jcis.2016.04.011.

Elmolla, E. S. & Chaudhuri, M. 2010 Effect of photo-Fenton operating conditions on the performance of photo-Fenton-SBR process for recalcitrant wastewater treatment. *Journal of Applied Sciences* **10**(24), 3236–3242. http://dx.doi.org/10.3923/jas.2010.3236.3242.

Gar Alalm, M. & Nasr, M. 2018 Artificial intelligence, regression model, and cost estimation for removal of chlorothalonil pesticide by activated carbon prepared from casuarina charcoal. *Sustainable Environment Research* **28**(3), 101–110. https://doi.org/10.1016/j.serj.2018.01.003.

Gar Alalm, M., Tawfik, A. & Ookawara, S. 2015 Degradation of four pharmaceuticals by solar photo-Fenton process: kinetics and costs estimation. *Journal of Environmental Chemical Engineering* **3**(1), 46–51. https://doi.org/10.1016/j.jece.2014.12.009.

Gar Alalm, M., Tawfik, A. & Ookawara, S. 2016 Solar photocatalytic degradation of phenol by $TiO_2$/AC prepared by temperature impregnation method. *Desalination and Water Treatment* **57**(2), 835–844. http://dx.doi.org/10.1080/19443994.2014.969319.

Gar Alalm, M., Samy, M., Ookawara, S. & Ohno, T. 2018 Immobilization of S-$TiO_2$ on reusable aluminum plates by polysiloxane for photocatalytic degradation of 2,4-dichlorophenol in water. *Journal of Water Process Engineering* **26**, 329–335. https://doi.org/10.1016/j.jwpe.2018.11.001.

Grassi, P., Drumm, F. C., Georgin, J., Franco, D. S. P., Foletto, E. L., Dotto, G. L. & Jahn, S. L. 2020 Water treatment plant sludge as iron source to catalyze a heterogeneous photo-Fenton reaction. *Environmental Technology & Innovation* **17**, 100544. https://doi.org/10.1016/j.eti.2019.100544.

Gümüş, D. & Akbal, F. 2016 Comparison of Fenton and electro-Fenton processes for oxidation of phenol. *Process Safety and Environmental Protection* **103**, 252–258. http://dx.doi.org/10.1016/j.psep.2016.07.008.

Jiang, Z., Wang, L., Lei, J., Liu, Y. & Zhang, J. 2019 Photo-Fenton degradation of phenol by CdS/rGO/$Fe^{2+}$ at natural pH with in situ-generated $H_2O_2$. *Applied Catalysis B: Environmental* **241**, 367–374. https://doi.org/10.1016/j.apcatb.2018.09.049.

Water Practice & Technology Vol 15 No 4
doi: 10.2166/wpt.2020.093

Novoselova, L. Y. 2016 Hematite nanopowder obtained from waste: iron-removal sludge. *Powder Technology* **287**, 364–372. http://dx.doi.org/10.1016/j.powtec.2015.10.020.

Omwene, P. I. & Kobya, M. 2018 Treatment of domestic wastewater phosphate by electrocoagulation using Fe and Al electrodes: a comparative study. *Process Safety and Environmental Protection* **116**, 34–51. http://dx.doi.org/10.1016/j.psep.2018.01.005.

Radwan, M., Gar Alalm, M. & Eletriby, H. 2018 Optimization and modeling of electro-Fenton process for treatment of phenolic wastewater using nickel and sacrificial stainless steel anodes. *Journal of Water Process Engineering* **22**, 155–162. https://doi.org/10.1016/j.jwpe.2018.02.003.

Rosales, E., Pazos, M. & Sanromán, M. A. 2012 Advances in the electro-Fenton process for remediation of recalcitrant organic compounds. *Chemical Engineering Technology* **35**(4), 609–617. https://doi.org/10.1002/ceat.201100321.

Saber, A., Hasheminejad, H., Taebi, A. & Ghaffari, G. 2014 Optimization of Fenton-based treatment of petroleum refinery wastewater with scrap iron using response surface methodology. *Applied Water Science* **4**, 283–290. doi:10.1007/s13201-013-0144-8.

Samy, M., Mossad, M. & El-Etriby, H. K. 2019 Synthesized nano titanium for methylene blue removal under various operational conditions. *Desalination and Water Treatment* **165**, 374–381. doi:10.5004/dwt.2019.24510.

Samy, M., Ibrahim, M. G., Gar Alalm, M. & Fujii, M. 2020a Effective photocatalytic degradation of sulfamethazine by CNTs/LaVO4 in suspension and dip coating modes. *Separation and Purification Technology* **235**, 116138. https://doi.org/10.1016/j.seppur.2019.116138.

Samy, M., Ibrahim, M. G., Gar Alalm, M., Fujii, M., Diab, K. E. & ElKady, M. 2020b Innovative photocatalytic reactor for the degradation of chlorpyrifos using a coated composite of Zrv2o7 and graphene nano-platelets. *Chemical Engineering Journal* **395**, 124974. https://doi.org/10.1016/j.cej.2020.124974.

Samy, M., Ibrahim, M. G., Gar Alalm, M., Fujii, M., Ookawara, S. & Ohno, T. 2020c Photocatalytic degradation of trimethoprim using S-$TiO_2$ and Ru/$WO_3$/$ZrO_2$ immobilized on reusable fixed plates. *Journal of Water Process Engineering* **33**, 101023. https://doi.org/10.1016/j.jwpe.2019.101023.

Samy, M., Ibrahim, M. G., Gar Alalm, M. & Fujii, M. 2020d MIL-53 (Al)/ ZnO coated plates with high photocatalytic activity for extended degradation of trimethoprim via novel photocatalytic reactor. *Separation and Purification Technology* **249**, 117173. https://doi.org/10.1016/j.seppur.2020.117173.

Sánchez-Rodríguez, D., Medrano, M. G. M., Remita, H. & Escobar-Barrios, V. 2018 Photocatalytic properties of BiOCl-$TiO_2$ composites for phenol photodegradation. *Journal of Environmental Chemical Engineering* **6**(2), 1601–1612. http://dx.doi.org/10.1016/j.jece.2018.01.061.

Shi, H., Yang, S., Han, C., Niu, Z., Li, H., Huang, X. & Ma, J. 2019 Fabrication of Ag/$Ag_3PO_4$/$WO_3$ ternary nanoparticles as superior photocatalyst for phenol degradation under visible light irradiation. *Solid State Sciences* **96**, 105967. https://doi.org/10.1016/j.solidstatesciences.2019.105967.

Shokri, A. 2018 Application of Sono–photo-Fenton process for degradation of phenol derivatives in petrochemical wastewater using full factorial design of experiment. *International Journal of Industrial Chemistry* **9**, 295–303. https://doi.org/10.1007/s40090-018-0159-y.

Tolba, A., Gar Alalm, M., Elsamadony, M., Mostafa, A., Afify, H. & Dionysiou, D. D. 2020 Modeling and optimization of heterogeneous Fenton-like and photo-Fenton processes using reusable $Fe_3O_4$-MWCNTs. *Process Safety and Environmental Protection* **128**, 273–283. https://doi.org/10.1016/j.psep.2019.06.011.

Wang, Y., Liang, M., Fang, J., Fu, J. & Chen, X. 2017 Visible-light photo-Fenton oxidation of phenol with rGO-*A*-FeOOH supported on Al-doped mesoporous silica (MCM-41) at neutral pH: performance and optimization of the catalyst. *Chemosphere* **182**, 468–476. http://dx.doi.org/10.1016/j.chemosphere.2017.05.037.

Wang, Y., Tian, H., Yu, Y. & Hu, C. 2018 Enhanced catalytic activity of *A*-FeOOH-rGO supported on active carbon fiber (ACF) for degradation of phenol and quinolone in the solar-Fenton system. *Chemosphere* **208**, 931–941. https://doi.org/10.1016/j.chemosphere.2018.06.007.

Wang, Y., Xi, Y., Tian, H., Fang, J., Quan, X. & Pei, Y. 2019 Effects of reaction conditions and liquid property on degradation of phenol by RGO/$\alpha$-FeOOH supported on Al-MCM catalyst in heterogeneous photo-Fenton system. *Catalysis Today* **335**, 460–467. https://doi.org/10.1016/j.cattod.2019.01.068.

Wei, X., Shao, S., Ding, X., Jiao, W. & Liu, Y. 2020 Degradation of phenol with heterogeneous catalytic ozonation enhanced by high gravity technology. *Journal of Cleaner Production* **248**, 119179. https://doi.org/10.1016/j.jclepro.2019.119179.

Xie, X., Hu, Y. & Cheng, H. 2016 Rapid degradation of p-arsanilic acid with simultaneous arsenic removal from aqueous solution using Fenton process. *Water Research* **89**, 59–67. http://dx.doi.org/10.1016/j.watres.2015.11.037.

Xu, X., Li, X., Li, X. & Li, H. 2009 Degradation of melatonin by UV, UV/$H_2O_2$, $Fe^{2+}$/$H_2O_2$ and UV/$Fe^{2+}$/$H_2O_2$ processes. *Separation and Purification Technology* **68**(2), 261–266. https://doi.org/10.1016/j.seppur.2009.05.013.

Zamora, R. M. R., Garcia, M. G., Gallardo, I. R., Rigas, F. & Duran-Moreno, A. 2006 Viability reduction of parasites (Ascaris spp.) in water with photo-Fenton reaction via response surface methodology. *Water Practice & Technology* **1**(2), wpt2006043. DOI: https://doi.org/10.2166/wpt.2006.043.